A numerical investigation of the interaction between debris flows and defense barriers

GIACOMO VICCIONE, SETTIMIO FERLISI
Dipartimento di Ingegneria Civile (DICIV)
Università di Salerno
C.U.G.Ri. - University Consortium for Research on Major Hazards
via Giovanni Paolo II, 132, 84084 Fisciano (SA)
ITALY
gviccion@unisa.it http://www.unisa.it/docenti/giacomoviccione/en/index

ELENA MARRA
Dipartimento di Ingegneria Civile (DICIV)
Università di Salerno
via Giovanni Paolo II, 132, 84084 Fisciano (SA)
ITALY

Abstract: - This paper presents some preliminary numerical results concerning the interaction between debris flows and defense barriers. Related simulations were carried out by employing a Computational Fluid Dynamics (CFD) commercial software. The approaching mass was treated as a single-phase equivalent fluid, obeying the generalized constitutive equation of Carreau.
Defense barriers are structures typically placed where significant mass movements, in terms of volumes or velocities involved, are expected. They are designed to withstand debris flow impacts as well as to contrast local forces exerted by debris on the invested surface. Classical design methodologies are mainly based on the application of available empirical formulations, such as those adopted in EUROCODE standards.
The proposed procedure yielded solicitations of magnitude usually lower than the corresponding obtained from classical approaches, hence potentially leading to the design of "less massive" works. Results, consisting of pressure fields and thrusts at the upfront barrier surface are discussed and compared with those ones derived from alternative methods.

Key-Words: - debris flows, defence barriers, mitigation, debris flow impact, fluid-structure interaction, numerical modelling, Computational Fluid Dynamics, CFD.

1 Introduction

Debris flows are channelized flow-like mass-movements involving loose unsorted material of low plasticity. They may also contain large objects as boulders or tree branches [1, 2]. Typically, their occurrence is related to the availability of material susceptible to be moved or triggered from area sources (the so called zero order basins, [3]), a significant soil moisture caused by heavy rain falls, a steep, confined, preexisting channel, an abundant supply of loose debris that make them growing by entrainment processes [4, 5], glacier melts or similar, a sparse vegetation caused by wildfire or deforestation. Such kind of phenomena are of particular interest to local authorities and researchers, owing their capability in travelling for long distances [6, 7] with attained maximum velocities up to 20 m/s, see [8] for predictions based on statistical methods, [9], reporting surface measurements taken by a fixed video camera, [10] about the estimation of expected maximum velocities, by means of dimensionless conveyance coefficients.

The above described features, the related unpredictability and the difficulties in designing effective countermeasures make debris flows extremely dangerous [11]. Every year many people are killed by them worldwide [12], not to mention related damages to infrastructures, human activities cultural heritage and livestock [13-19], see the free OFDA/CRED International Disaster Database [20] for an overall view.

Attempting to forecasting triggering and propagating processes in terms of physical characteristics and expected magnitude, see for instance [21-23], is therefore of considerable interest, e.g. in land-use management based on hazard mappings definition [24-26].

Debris flow hazard can be mitigated by allowing the approaching mass impacting [27, 28] on structural works. They may consist of defense barriers – flexible or rigid – to be placed where such events are expected to take place. Flexible types [29-31], as net barriers, are installed in recent years in small basins for containing moderate debris flow events.

This work refers about rigid barriers [32-34], such as concrete works, in which elasticity effects are assumed negligible when the interaction between the approaching mass and structure takes place. Still, the related phenomenon is quite difficult to model, due to the physical and rheological characteristics [35] of interacting mass, composed – in the general case – by a wet mixture of sediments of different size. In addition, in literature there are different rheological models [7, 36-38], empirical or theoretical based, describing the stress-strain relationship. Empirical models, such as those represented by power laws, are basically derived by regressing experimental data. Theoretical models are derived from the application of fundamental physical concepts. The identification of the correct one is not an easy task. Just to mention some main issues, debris flow behaviour can vary from nearly rigid to liquefied as a consequence of temporal and spatial gradients associated to the pore-fluid pressure and mixture agitation [39]. The volume fraction of fine sediments trapped in the interstitial fluid affects the dynamic viscosity [40] along with the local rate of deformation, size distribution and mineralogical properties. Anyway, most of the available literature, gathering field and laboratory investigations, concerning at least muddy debris flows, indicates that they can be outlined by linear (Bingham) or nonlinear (Herschel-Bulkley) viscoplastic models [41-43].

Having in mind all the above issues, a numerical investigation of exerted solicitation on rigid defense barriers is here proposed. The propagating mass is treated as a single-phase equivalent fluid, that is liquid and solid phases are "merged" into a single phase medium.

2 Methodology

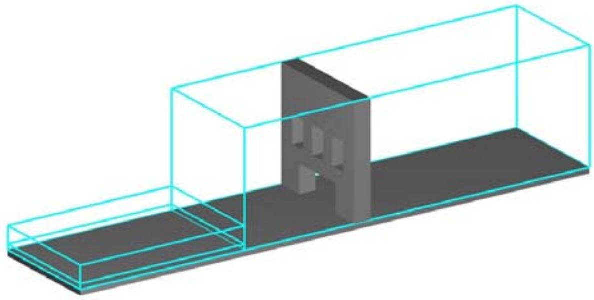

Fig. 1. Schematic view of the assumed geometry.

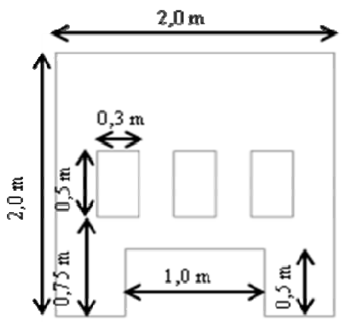

Fig. 2. Upfront view of the implemented barrier.

Here, we describe the way numerical results related to the interaction between an approaching fluid mass and a defensive barrier are obtained. Assumed geometry and boundary conditions are described in section 2.1. Computations were carried out by means of the Flow 3D ® software (see section 2.2), Ruling equations are discussed in section 2.3.

2.1 Model set up

An open channel flow is set upstream, imposing a constant hydrograph in time, with prefixed values of velocity *V*_in and height *h*_in. The generated mass flow of specific weight γ=1600kg/m^3, first propagates over the channel, then impacts against the upfront surface of a defence barrier (Fig. 1). For computational purposes, the rectangular channel is assumed 9.30m long and 2m wide. The barrier is placed 5m from the upstream end where boundary conditions are given.

Sixteen scenarios are considered, corresponding to the combination of four velocities *V*_in (1m/s, 2m/s, 5m/s e 10m/s) and flow stages *h*_in (0.1 m, 0.2m , 0.5m e 1.0m). The outflow condition is assumed at the downstream end instead.

Geometry is assembled in a CAD environment then converted in the STereo Lithography interface (stl) format, a standard which can be provided to the Flow-3D solver as input file. A sketch of the analyzed barrier is shown in Fig. 2.

ISBN: 978-1-61804-314-6

2.2 The Flow 3D model

The Flow-3D solver [44] is a CFD commercial software based on a Finite Volume formulation of the ruling equations in the Eulerian framework. Free surfaces and interfaces are solved with the volume of fraction (VOF) method [45] and the Fractional Area/Volume Obstacle Representation (FAVOR). Velocity and pressure fields are coupled by using the time-advanced velocities in the continuity equations and time-advanced pressures in the momentum equation. Ruling equations are provided in the next section 2.3.

Temporal integration is performed with a two-step momentum predictor-continuity corrector procedure. In carrying out numerical tests, the corrector step makes use of a weakly compressible approach, whereby in the continuity equation a variable density mass flow is considered and the compressibility is simulated through a linear law which links the density variation to the pressure increase. No additional dissipation term is included in the momentum equation, so this approach is valid for low Mach numbers and is consistent with the acoustical approximation in much of the current literature. The model has been validated over the years for similar operating conditions for wave impact problems, see for instance [46-49]

The computational domain is discretized by considering at most three spatial sub-regions (see Fig. 1) featuring a specific cell size (coarse to fine grid resolution from left to right side). This is basically due to the need to speed up simulations. In addition, spatial discretization is performed only where the fluid is expected to take place. All tests, shown in the following, have been carried out by assuming a single-phase equivalent fluid with reference density $\rho_0 = 2000$ kg/m^3.

2.3 Governing equations

Flow-3D® package is able to simulate pseudo-plastic fluid flows by embedding the following stress-strain relationship expressed in tensor notation

$$\underline{\underline{\tau}} = \mu(\dot{\gamma})\underline{\underline{D}} \tag{1}$$

in the momentum balance equation

$$\rho\frac{\partial \underline{v}}{\partial t} + \rho\underline{v}\underline{\nabla} \bullet \underline{v} = \underline{\nabla} p + \underline{\nabla} \bullet \underline{\underline{\tau}} \tag{2}$$

where the symbol "●" stands for the scalar product.

The meaning of symbols inside eqs. (1) and (2) follows:

- $\underline{\underline{\tau}}$ is the stress tensor; $\underline{\nabla}$ is the nabla operator
- $\dot{\gamma}$ is the shear rate given by

$$\dot{\gamma} = \sqrt{\frac{1}{2} D_{ij} D_{ij}} \tag{3}$$

(Einstein notation is assumed here and in the following. Repeated indices imply the implicit summation);

- D_{ij} correspond to the matrix components of the rate of deformation tensor $\underline{\underline{D}}$;
- ρ is the variable density;
- $\underline{v}$ and p are the fluid velocity and pressure respectively;
- the dynamic viscosity μ is computed by applying the Carreau-Yasuda model

$$\mu = \mu_0 + (\mu_0 - \mu_{\inf})\left[1 + (\lambda\dot{\gamma})^2\right]^{\frac{n-1}{2}} \tag{4}$$

where $\mu_0 = 0.01$ Pa·s and $\mu_{\inf} = 0$ are the zero and infinite shear rate limit viscosities respectively, λ = 1s is the relaxation time constant and n=0.8 is the power law index. Numerical values of above parameters were obtained after calibration, comparing travelled distances with corresponding ones from a test case analized in [50]. Model closure is obtained by solving eq. (2) together with the continuity equation, next expressed in the general form

$$\frac{\partial \rho}{\partial t} + \underline{\nabla} \bullet (\rho\underline{v}) = 0 \tag{5}$$

3. Results

In this chapter numerical results in terms of propagating velocities, energy loss at the barrier, impact pressure distribution and hydrodynamic forces, are provided and discussed.

3.1 Mean spatial velocity on channel upstream

The mean velocity modulus *V*_ws, (ws stands for "wet surface" whereas capital word *V* is referred to the averaging extracting) of the propagating mass, travelling over the upstream channel (5m long), is obtained on five vertical cross-sections, equally spaced out. The final one matches the upfront surface of the barrier. On such location, the mean velocity is also computed with reference to the

ISBN: 978-1-61804-314-6

permeable surface, yielding the variable *V*_ps (sketched with a bigger marker in the next Fig. 3.

Average *V*_ws values, for each wet section Σ_i, i=1,…5, were obtained by weighting local velocities v_j with the wet surface of cells, as some of them might not be completely filled

$$V\_ws = \frac{f_j \cdot v_j \cdot A_j}{f_j \cdot A_j} \tag{6}$$

where *f*, *v* and *A* are the fluid fraction, the velocity modulus and the area of j-th cell (thus $f_j A_j = \Sigma_i$), respectively. Implicit summation is referred only to cells, partially or completely wet.

Spatial velocity distribution are next shown in Fig. 3. Sub-plots refer to the initial fluid level *h*_in fixed at the upstream boundary condition. Curves on each sub-plot then correspond to the initial fluid velocity *V*_in (see section 2.1 for assigned values).

As can be seen, the propagating mass accelerates moving downstream. This is basically due to the conversion of the initial mechanical energy content (potential plus kinetic) into kinetic energy. The higher is *h*_in, the higher is the rate of displacement. Despite the presence of flow resistances, in the worst case represented by *h*_in=1.0m and V_in=10m/s (uppermost curve in subplot (d), Fig. 3), the mass gains 20% more velocity (1-12/10)x100. The presence of the barrier implied a velocity attenuation on *V*_ws instead, as can be seen from subplots (a), (b) and (c). Keeping *h*_in fixed, the higher is *V*_in, the lower is the reduction, that is a minor deceleration takes place. The reduction takes no more place in the worst case. This aspect is further enhanced in the next section 3.2.

A comparison of gain velocities at the final wet section 5 is provided in Fig. 4. Graph is expressed in terms of dimensionless quantities *V*_ws/*V*_in and *h*_in/*H*_ds, being *H*_ds=2.0m the height of the adopted defense structure, see Fig. 2. The scaled velocity built this way, straightly established whether the flow accelerates (>1) or decelerates (<1) for any given boundary condition.

Quite interestingly, it is not the general couple (*h*_in, *V*_in_max=10m/s) that returns the maximum flow acceleration. For instance, the case (*h*_in_max=1,0m, *V*_in_max=10m/s), cross marker on the right side of Fig. 4, yields the minimum velocity increase whereas the maximum is given by the couple (*h*_in_max=1,0m, *V*_in =1m/s), star marker. In other terms, when the initial kinetic energy content is predominant, the initial potential energy content is negligibly converted and the fluid travels at approximately the same velocity (see cross

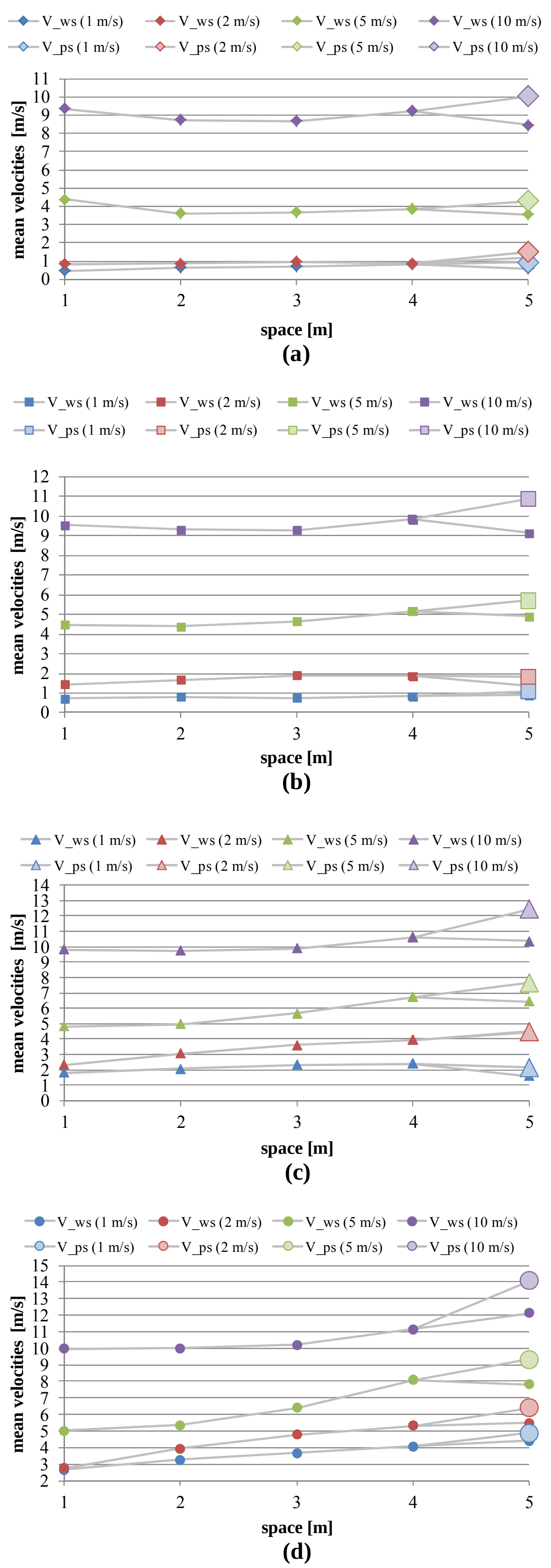

Fig. 3. Mean spatial velocity on channel upstream. (a) h_in=0.1m, (b) h_in=0.2m, (c) h_in=0.5m, (d) h_in=1.0m.

ISBN: 978-1-61804-314-6

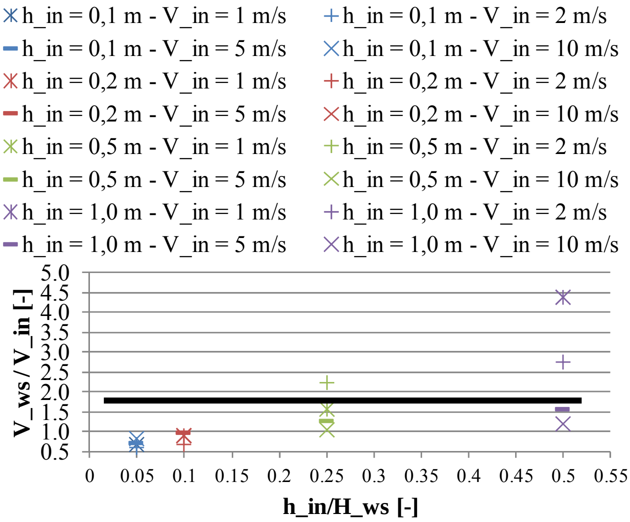

Fig. 4. Dimensionless velocities V_ws/V_in soon before the upfront wall of the barrier vs the dimensionless spatial scale h_in/H_ds. Markers above thick line indicates that the fluid globally accelerates on channel upstream.

markers close to the horizontal bold line V_ws/V_in=1.0).

3.2 Energy loss at the barrier

We consider the application of the Bernoulli theorem

$$\Delta H = \left(\bar{z}_u + \frac{\bar{p}_u}{\gamma}\right) + \left(\frac{1}{\Sigma_{ws\_u}}\right)\int_{\Sigma ws\_u} \frac{v_u^2}{2g} d\sigma + \qquad (7)$$
$$-\left[\left(\bar{z}_d + \frac{\bar{p}_d}{\gamma}\right) + \left(\frac{1}{\Sigma_{ws\_d}}\right)\int_{\Sigma ws\_d} \frac{v_d^2}{2g} d\sigma\right]$$

when stationary conditions occurred. Steady states are detected as in [51].

Eq. (7) is applied to a control volume comprehending the defensive barrier. Upstream (u) and downstream (d) permeable surfaces were chosen so that the flow was about to be one-dimensional through them (0.50m from solid surfaces in order to neglect distribute losses). The meaning of symbols is as follows: Σ_{ws} is the wet surface, $\bar{z}$ is the z-coordinate (from the bottom) of its barycenter, $\bar{p}$ is the average pressure, computed as in eq. (6), v is the local velocity.

The same eq. (7) was discretized as follows:

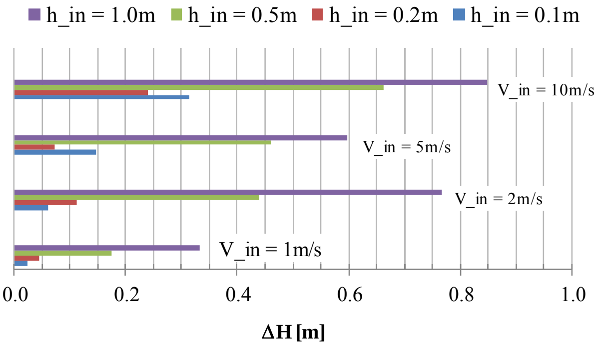

Fig. 5 Energy loss at the barrier computed by eq. 8 for h_in=0.1m-1.0m; V_in=1m/s-10m/s.

$$\Delta H = \left(\bar{z}_u + \frac{\bar{p}_u}{\gamma}\right) + \frac{1}{2g \cdot \Sigma_{ws\_u}} v_{u,j}^2 \cdot \left(f_{u,j} \cdot A_{u,j}\right) + \qquad (8)$$
$$-\left[\left(\bar{z}_d + \frac{\bar{p}_d}{\gamma}\right) + \frac{1}{2g \cdot \Sigma_{ws\_d}} v_{d,j}^2 \cdot \left(f_{d,j} \cdot A_{d,j}\right)\right]$$

being $f_{k,j} \cdot A_{k,j} = \Sigma_{ws\_k}$, k=u,d.

Figure 5 yields ΔH values as computed by eq. (8), for each case investigated. As can be observed, the energy loss ΔH is not always monotone with the initial flow velocity *V_in*. In particular, for *h_in_max* =1.0m there is a relative minimum, corresponding to *V_in*=5m/s. Anyway, maximum ΔH values always correspond to *V_in_max*=10m/s.

3.3 Impact Pressure distribution at the upfront surface of the barrier

This section is intended to show the non-linear behaviour - for high propagating velocities - of the pressure distribution as the impact takes place. When the flow comes in contact with the solid surface, there is locally an abrupt increase in the pressure magnitude. A first pressure peak p_m is then reached. A secondary peak p_s, lower in magnitude may then appear. A graph of pressure vs time then looks like a ‘church steeple’ profile (Fig. 6).

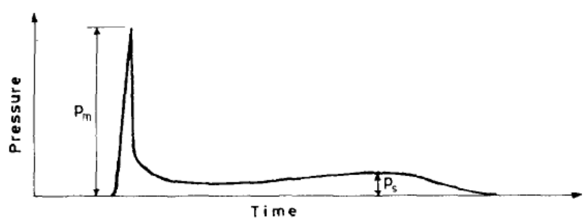

Fig. 6. Temporal evolution of the pressure field.

ISBN: 978-1-61804-314-6

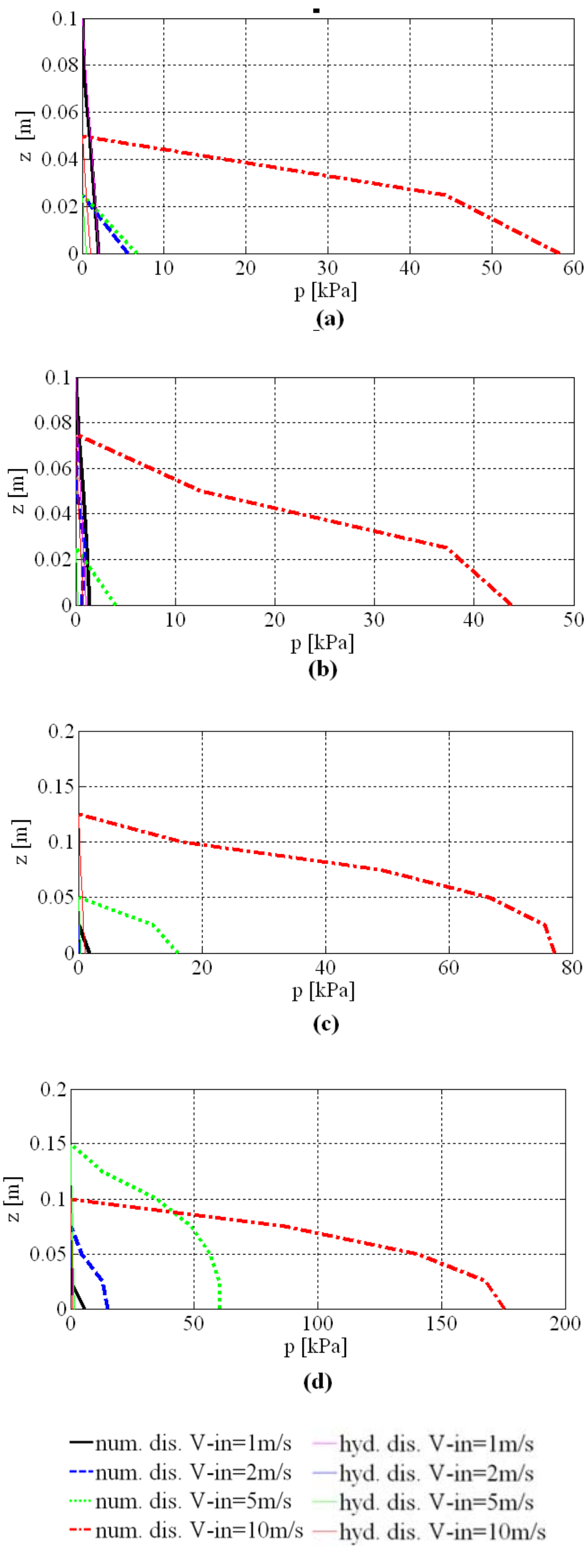

Fig. 7. Numerical pressure distribution profiles along verticals where the maximum arises. (a) h_in=0.1m, (b) h_in=0.2m, (c) h_in=0.5m, (d) h_in=1.0m. Hydrostatic distributions are shown as well for comparison, although not readable for sub-plots (c) and (d) as they overlap with the vertical axis.

In the above Fig. 7, spatial pressure trends along the vertical direction where the maximum occurs are provided. Hydrostatic distributions *p*_id(z)=γ(h_ws-z), being γ the specific weigth, h_ws the fluid depth at the barrier on the same vertical direction, are given as well for comparison.

As can be observed, the higher is *V*_in, the higher is the gap between numerical and hydrostatic distributions. This aspect turns out to be significant in the evaluation of the amplification factor α of the dynamic pressure p_d, given by empirical relationships, such as:

$$p_{\mathrm{d}} = \alpha \cdot \gamma \cdot h\_\mathrm{ws} \qquad (9)$$

α is commonly chosen between 3 and 5 in the engineering practice.

Maximum pressure increases monotonically with *V*_in as can be expected, not with *h*_in as can be observed from sub-plot (b) of Fig. 7. Keeping *V*_in_max=10m/s fixed (dash-dotted red lines), the maximum pressure is minimized for *h*_in=0.2m (p_{max}=44kPa), being comprised between the corresponding values for h_in=0.1m (p_{max}=58kPa, sub-plot (a)) and h_in=5m (p_{max}=77kPa, sub-plot (c)). This aspect turns out to be significant as the pressure main peak is not only related to the velocity of the approaching mass flow. More precisely it depends on the combination of velocity and height (i.e. momentum, in a single word), at the upfront of the propagating domain, soon before the impact.

3.4 Hydrodynamic force on the upfront surface of the barrier

The evaluation of hydrodynamic forces acting on barriers is of primary interest in common practice. In facts, integral solicitations commonly appear in a global equilibrium. Here we refer to two particular conditions: the first one is related to a short period soon after the impact instant. The second one is referred to the period of time needed for the achievement of steady conditions.

The aim is to compare forces corresponding to the above cited as well as to assess to what extend impact forces can be neglected when compared with steady forces. In any case, the hydrodynamic force S is evaluated by summing pressure forces applied on the wet contact surface as follows:

$$S = p_{\mathrm{j}} \cdot f_{\mathrm{j}} \cdot A_{\mathrm{j}} \qquad (10)$$

$f_j < 1$ occurs in correspondence of partially wetted cells, $f_j = 1$ otherwise.

ISBN: 978-1-61804-314-6

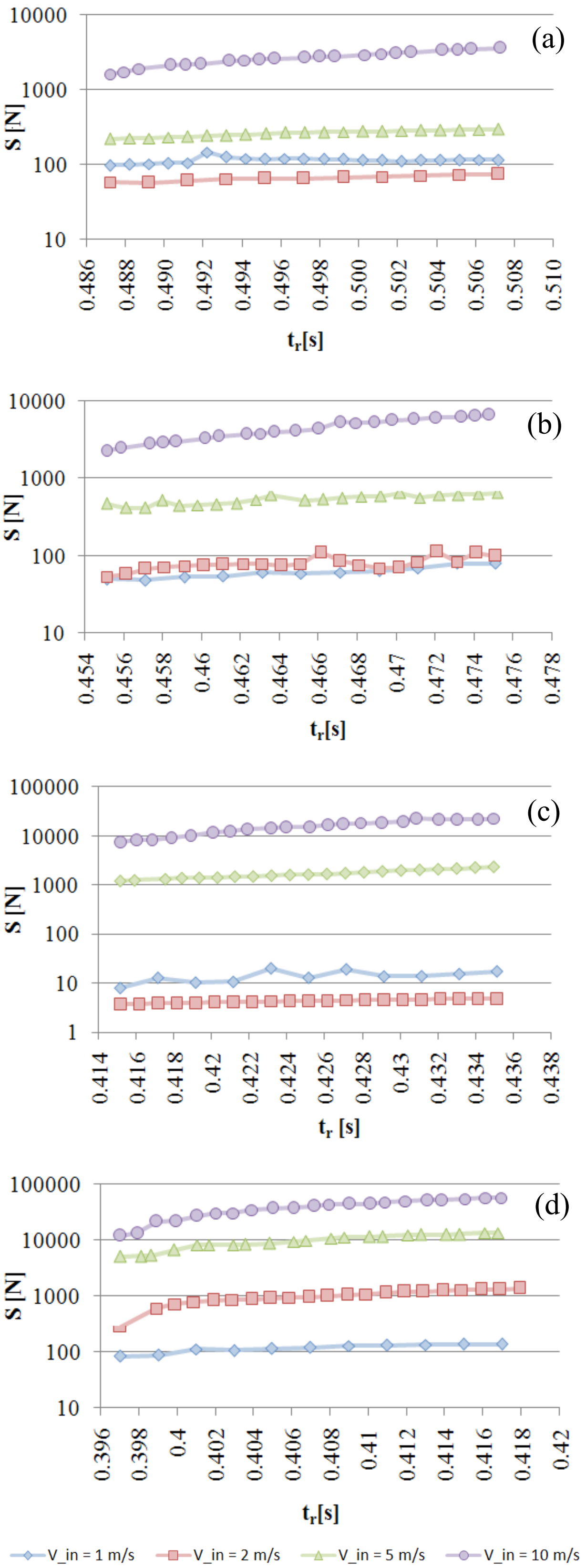

Fig. 8. Temporal variation of the hydrodynamic force S at the wall. The independent variable t_r denotes the time respect the impact instant of the slowing flowin mass. (a) h_in=0.1m, (b) h_in=0.2m, (c) h_in=0.5m, (d) h_in=1.0m.

- *Trends soon after the flow impact*

As the impact takes place, we do not observe a quick increase in the hydrodynamic force as occur for local pressures instead (see section 3.3). This is basically due to the fact that the force is obtained by an integral condition over the entire wet surface.

Fig. 8 shows aligned temporal trends over a short period of time, measured respect the impact instant of the slowest flowing mass, which always occur for *V*_in=1m/s.

Despite a base-10 log scale is used for the dependent variable, It is quite evident the corresponding smooth variation of $S(t_r)$.

It is interesting to observe that the force is not always monotone with the initial velocity *V*_in. In particular this can be noted in sub plots (a) and (c) of Fig. 8 where the force trend for *V*_in=0.2m/s is below the corresponding one for *V*_in=0.1m/s. This can be justified on the basis of the kinematic conditions of the moving mass as the impact takes place. As general behavior, when the Froude number increases (let it assumed in terms of the front wave, Fr = $V\_ws/(g\cdot h\_ws)^{0.5}$, being g the gravity acceleration, *V*_ws and *h*_ws the mean velocity and fluid level of the approaching mass, almost in contact with the upfront barrier), the fluid mass become less prone to be curved at the surface (at least for some instants) hence yielding lower forces but higher local pressures at the wall. Such a circumstance is equivalent to the movement of supercritical flows which is only dependent on upstream boundary conditions.

- *Trends over a period of time, needed for the achievement of steady conditions*

Here, hydrodynamic force trends on a wider period needed to reach steady flow conditions are deducted. For computational reasons we regressed the available trends in order to infer on the final steady values of the force.

Numerical results are shown in Fig. 9. As can be observed, this time the applied force is always monotone with the initial velocity *V*_in. In addition, it exhibits a maximum, see sub plot (a) for *V*_in=10m/s, sub plots (c) and (d) for *V*_in=5m/s. Such a behavior is related to the kinematic of the incident wave. For higher velocity values, i.e. for higher Froude numbers, the impinging wave determines a maximum solicitation, then a relative relaxation occurs.

- *Comparison of hydrodynamic forces*

ISBN: 978-1-61804-314-6

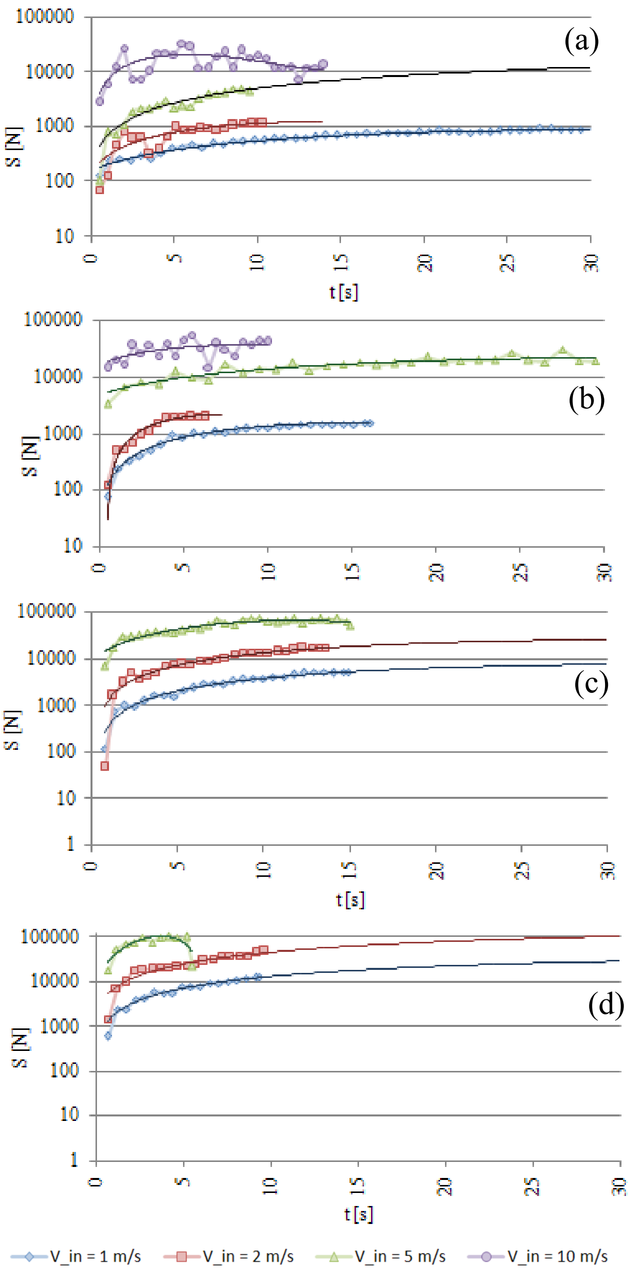

Fig. 9. Temporal variation of the hydrodynamic force S at the wall. Here, the independent variable t, denotes the absolute time. (a) h_in=0.1m, (b) h_in=0.2m, (c) h_in=0.5m, (d) h_in=1.0m.

In Table 1 hydrodynamic forces are provided for two conditions:

- as the impact takes place (maximum force S_i over a subsequent short period of time);
- as steady conditions are reached (final force S_s or relative maximum, when occurs).

A comparison is then made in Table 2 by computing the ratio between S_i and S_s.

Table 1. Numerical exerted forces [kN] at the barrier.

	*V*_in=1m/s		*V*_in=2m/s		*V*_in=5m/s		*V*_in=10m/s	
	S_i	S_s	S_i	S_s	S_i	S_s	S_i	S_s
h_in=0.1m	0.12	.99	0.08	3.03	0.30	14.63	3.64	15.5
h_in=0.2m	0.08	2.91	0.11	10.73	0.64	24.77	6.50	42.00
h_in=0.5m	0.03	9.05	0.01	39.65	2.33	88.09	22.77	n.a.
h_in=1.0m	0.24	39.55	1.36	94.23	13.40	102.7	57.40	n.a.

Table 2. Ratio between S_i and S_s.

	*V*_in=1m/s	*V*_in=2m/s	*V*_in=5m/s	*V*_in=10m/s
	S_i/S_s [%]	S_i/S_s [%]	S_i/S_s [%]	S_i/S_s [%]
h_in=0.1m	12.1	2.6	2.1	23.5
h_in=0.2m	2.7	1.0	2.6	15.5
h_in=0.5m	0.3	0.0	2.6	n.a.
h_in=1.0m	0.6	1.4	13.0	n.a.

As can be observed, integral solicitations occurred when the impact took place were always lower or much lower than corresponding ones exerting on the barrier when steady conditions were attained.

Anyway, it is worth observing that for some couples (*h*_in, *V*_in) the ratio S_i / S_s was of the order of tens percent, i.e. not negligible. The worst case recorded arisen for the couple (h_in_min=0.1m, V_in_max=10m/s). Such a circumstance suggest that low, fast travelling flowing masses needs to be assessed when the impact takes place.

4. Conclusions

In this work, some preliminary numerical results concerning the interaction between debris flows and defence barriers were presented. The moving mass was treated as a single equivalent fluid obeying the Carreau constitutive equation whereas the solid interface as a rigid surface. Fluid propagation and energy loss at the barrier were assessed in terms of

ISBN: 978-1-61804-314-6

the imposed boundary conditions at the upstream cross section of the channel.
Non linear pressure distributions along the vertical direction were deducted for high propagating velocities. Significant gap with the hydrostatic distribution was deduced as well.
Hydrodynamic forces were determined by summating local pressure forces over the wet surface of the barrier. We proved that, under certain conditions, global solicitations that arise soon after the impact were comparable with the corresponding ones, obtained when steady conditions were attained.

Acknowledgments

This work was financially supported by the National Research Project (PRIN) 2010-2011 on "Landslide risk mitigation through sustainable countermeasures" (CUP D41J12000460001, Scientific Coordinator: Prof. Leonardo Cascini).

References:

[1] Costa J. E., Physical geomorphology of debris flows, In: Costa J. E. and Fleischer P. J. (eds), *Developments and Applications of Geomorphology*, Springer, Berlin, Germany, pp. 268–317, 1984.
[2] Takahashi T., *Debris Flow*, IAHR Monograph Series, Balkema, Rotterdam, The Netherlands, 1991.
[3] Guida D., The role of the zero-order basins in flowslide-debris flows occurrence and recurrence in Campania (Italy). In: *Fast slope movements - Prediction and Prevention for risk mitigation*, Vol. 1, 2003, pp. 255-267.
[4] Reid M. E., Iverson R. M., Logan M., LaHusen R. G., Godt J. W. and Griswold J. P., Entrainment of bed sediment by debris flows: results from large-scale experiments, Italian Journal of Engineering Geology and Environment, 2011, pp. 367-374.
[5] Cuomo S., Pastor M., Cascini L. and Castorino G. C., Interplay of rheology and entrainment in debris avalanches: a numerical study. *Canadian Geotechnical Journal*, 2014, pp. 1-13, ISSN:0008-3674.
[6] Iverson R. M., 1997, The physics of debris flows, *Rev. Geophys.*, Vol. 35, 1997, pp. 245–296.
[7] Rickenmann D. Empirical relationships for debris flows, *Natural Hazards*, Vol. 19, 1999, pp. 47-77.
[8] Prochaska A. B., Santi P. M., Higgins J. D. and Cannon S. H., A study of methods to estimate debris flow velocity, *Landslides*, Vol. 5, 2008, pp. 431-444.
[9] Arattano M. and Grattoni P., Using a fixed video camera to measure debris-flow surface velocity. In: Wieczorek G.F., Naeser N.D. (eds) *Debris-flow hazards mitigation: mechanics, prediction, and assessment. Proceedings of the second international conference*. AA Balkema, Rotterdam, 2000, pp. 273–281.
[10] Gregoretti C., Estimation of the maximum velocity of a surge of debris flow propagating along an open channel. *International Symposium Interpraevent 2000*. Villach, 2000, pp. 397-409.
[11] Hungr O. and Jakob M., *Debris-flow Hazards and Related Phenomena*. Springer, Berlin, 2005.
[12] Cascini L., Ferlisi S. and Vitolo E., Societal risk due to landslides in the Campania region (Southern Italy). In: *Landslides and Engineered Slopes. From the Past to the Future*, London (U.K.), Taylor and Francis Group, 2, 2008, pp.1893-1898.
[13] Faella C. and Nigro E., Dynamic impact of the debris flows on the constructions during the hydrogeological disaster in Campania 1998: Failure mechanical models and evaluation of the impact velocity. In: *Fast slope movements-prediction and prevention for risk mitigation*, Napoli 11-13 maggio 2003, Vol.1, 2003, pp.179-186.
[14] Heumader J., The catastrophic avalanche disasters of Galtür and Valzur on the 23. and 24 of February 1999 in the Paznaun valley / Tyrol., *International Symposium Interpraevent 2000*. Villach, 2000, pp. 397-409.
[15] Hübl J., Kienholz H. and Loipersberger A., DOMODIS - Documentation of Mountain Disasters, State of Discussion in the European Mountain Areas. Vienna, 2002
[16] Hübl J., Habersack H., Kienholz H., Agner P., Ganahl E., Moser M., Scheidl C., Kerschbaumsteiner W. and Schmid F., Disaster Information System of Alpine Regions (DIS-ALP): Methodik Teil 1. IAN Report 101. Vienna, 2006.
[17] Hurlimann M., Copons R. and Altimir J., Detailed debris flow hazard assessment in Andorra, a multidisciplinary approach, *Geomorphology*, Vol. 78, 2006, pp. 359 – 372.
[18] Metternicht G., Hurni L. and Gogu R., Remote sensing of landslides: An analysis of the potential contribution to geo-spatial systems for

hazard assessment in mountainous environments, *Remote Sensing of Environment*, Vol. 98(2), 2005, pp. 284-303
[19] Pfurtscheller C. and Thieken A. H., The costs of natural hazards in alpine environments. Current practice, end-user needs and recommendations, *International Symposium Interpraevent 2012* – Grenoble / France, 2012, pp. 1045 – 1054.
[20] Guha-Sapir D., Below R. and Hoyois P., EM-DAT: International Disaster Database – www.emdat.be – Université Catholique de Louvain – Brussels – Belgium.
[21] Fraccarollo L. and Papa M. N., Numerical simulation of real debris-flow events, *Phys. Chem. Earth, Part B*, Vol. 25(9), 2000, pp. 757-763.
[22] Viccione G. and Bovolin V., Simulating Triggering and Evolution of Debris-Flows with Smoothed Particle Hydrodynamics (SPH). *Italian Journal of Engineering Geology and Environment*, 2011, pp. 523-532.
[23] Cascini L., Cuomo S., Pastor M., Sorbino G. and Piciullo L., SPH run-out modelling of channelised landslides of the flow type. *Geomorphology*, Vol. 214. 2014, pp. 502-513 ISSN:0169-555X.
[24] Corominas J., van Westen C., Frattini P., Cascini L., Malet J.-P., Fotopoulou S., Catani F., Van Den Eeckhaut M., Mavrouli O., Agliardi F., Pitilakis K., Winter M.G., Pastor M., Ferlisi S., Tofani V., Hervàs J., Smith J.T., Recommendations for the quantitative analysis of landslide risk. *Bulletin of Engineering Geology and the Environment*, Vol. 73(2), 2014, pp. 209-263
[25] Bertoldi G, D'Agostino V. and McArdell B. W., An integrated method for debris flow hazard mapping using 2d runout models, In: 12th *International Symposium Interpraevent 2012* – Grenoble / France, 2012, pp. 435-446.
[26] Fell R., Corominas J., Bonnard C. H., Cascini L., Leroi E. and Savage B., Guidelines for landslide susceptibility, hazard and risk zoning for land use planning. *Engineering Geology*, Vol. 102, 2008, pp. 85-98.
[27] Armanini A., On the Dynamic Impact of Debris Flows. In Armanini A. and Michiue M., editors, Recent Developments on Debris Flows, Springer Berlin Heidelberg, 1990. pp. 208–226.
[28] Hübl J., Suda J., Proske D., Kaitna R. and Scheidl C., Debris Flow Impact Estimation. In *International Symposium on Water Management and Hydraulic Engineering*, Ohrid/Macedonia, 2009, pp. 137–148.
[29] Rickenmann D., Estimation of debris flow impact on flexible wire rope barriers. *Internal report WSL*, Birmensdorf, 2001.
[30] Volkwein A., Wendeler C. and Guasti G., Design of flexible debris flow barriers, *Journal of Engineering Geology and Environment*, 2011, pp. 1093-1100.
[31] Brighenti R., Segalini A. and Ferrero A. M.., Debris flow hazard mitigation: A simplified analytical model for the design of flexible barriers. *Computers and Geotechnics*, Vol. 54, 2013, pp. 1–15.
[32] Hungr O., Morgan G. C. and Kellerhals R., Quantitative analysis of debris torrent hazard for design of remedial measures, *Canadian Geotech. J.*, Vol. 21, 1984, pp. 663–677.
[33] Armanini, A. and Scotton, P., 1993, On the dynamic impact of a debris flow on structures, *Proceedings of XXV Congress IAHR*, Tokyo (Tech. Sess. B, III), pp. 203–210.
[34] Canelli L., A. Ferrero M., Migliazza M. and Segalini A.. Debris flow risk mitigation by the means of rigid and flexible barriers – experimental tests and impact analysis, *Natural Hazards and Earth System Science*, Vol. 12(5), 2012, pp. 1693–1699.
[35] Kaitna R., Rickenmann D. and Schatzmann M., Experimental study on rheologic behaviour of debris flow material, *Acta Geotechnica*, Vol. 2(2), 2007, pp. 71–85.
[36] Coussot P., Laigle D., Arattano M., Deganutti A. and Marchi L., Direct determination of rheological characteristics of debris flow, J. Hydraul. Eng., Vol. 124(8), 1998, pp. 865-868.
[37] Hübl J. and H. Steinwendtner, Estimation of rheological properties of viscous debris flows using a belt conveyor, *Phys. Chem. Earth, Part B*, 25(9), 2009, pp. 751-755.
[38] Genovese M., Viccione G., Rossi F., Guida D. and Lenza T.L.L., 2014. Using the Sodium Carboxymethylcellulose (CMC) as viscosity modifier to model the interstitial fluid in laboratory debris flows, in: G. Viccione, C. Guarnaccia (Editors), *Latest Trends in Engineering Mechanics, Structures, Engineering Geology, Proceedings of the 7th International Conference on Engineering Mechanics, Structures, Engineering Geology (EMESEG '14)*, Salerno, Italy, June 3-5, Vol. 26, 2014, pp. 179 -186.
[39] Iverson R.M., The debris-flow rheology myth. In Rickenmann D. & Chen C.-L., (Editors), *3rd International Conference on Debris-flow Hazard Mitigation: Mechanics, Prediction and Assessment*, Vol. 1, 2003, pp. 303-314.

[40] Major J. J. and Pierson T. C., Debris flow rheology: experimental analysis of fine-grained slurries, *Wat. Resour. Res.*, Vol. 28(3), 1992, pp. 841–857.
[41] Johnson, A. M., *Physical Processes in Geology*. Freeman, San Francisco, Calif. 1970
[42] O' Brien, J. S. and Julien, P. Y., Laboratory analysis of mudlfow properties, *J. Hydraul. Engrg.*, ASCE, Vol. 114(8), 1988, pp. 877-887.
[43] Locat, J., Normalized rheological behaviour of muds and their flow properties in a pseudoplastic regime, In: *Debris-flow hazard mitigation: mechanics, prediction, and assesment, Proc., First Int. Conf., ASCE*, 1997, pp. 260-269
[44] FLOW 3D, 2010, User Manual Version 9.4, Flow Science, Inc., Santa Fe.
[45] Hirt C. W. and Nichols B. D., Volume of fluid (VOF) method for the dynamics of free boundaries, *Journal Comp. Physics*, Vol. 39, 1981, pp. 201-225.
[46] Cavallaro L., Dentale F., Donnarumma G., Foti E., Musumeci R. E., Pugliese Carratelli E., Rubble Mound Breakwater Overtopping: Estimation of the reliability of a 3D Numerical Simulation, *ICCE 2012 International Conference on Coastal Engineering*, Santander, Spain, 2012
[47] Dentale F., Donnarumma G. and Pugliese Carratelli E., Wave run up and reflection on tridimensional virtual breakwater, *Journal of Hydrogeology & Hydrologic Engineering*, 2012, http://dx.doi.org/10.4172/jhhe.1000102.
[48] Dentale F., Donnarumma G. and Pugliese Carratelli E., 2014a, Simulation of flow within armour blocks in a breakwater. *Journal of Coastal Research*, Vol. 30(3), pp. 528–536.
[49] Dentale F., Donnarumma G. and Pugliese Carratelli E., Numerical wave interaction with tetrapods breakwater, *International journal of naval architecture and ocean engineering*, Vol. 6, 2014b, pp. 1-13, ISSN:2092-6782.
[50] Ghilardi, P., Natale, L. and Savi, F., Experimental investigation and mathematical simulation of debris-flow runout distance and deposition area, *3rd International Conference on Debris-Flow Hazards Mitigation: Mechanics, Prediction, and Assessment*, Davos, Switzerland, 2003, pp. 601-610
[51] Viccione G., Spiniello D., Zarra T and Naddeo V., Fluid Dynamic Simulation of Odour Measurement Chamber. *Chemical engineering transactions*, Vol. 40, 2014, pp. 109-114.